

# River profile evolution by plucking in lithologically heterogeneous landscapes: Uniform uplift vs. tilting

Emmanuel J. Gabet\* 

Department of Geology, San Jose State University, San Jose, CA 95192, USA

Received 25 October 2019; Revised 28 January 2020; Accepted 30 January 2020

\*Correspondence to: E. J. Gabet, Department of Geology, San Jose State University, San Jose, CA 95192, USA. E-mail: manny.gabet@sjsu.edu

# ESPL

Earth Surface Processes and Landforms

**ABSTRACT:** Recent studies provide a theoretical framework for understanding the incision of bedrock rivers by plucking. These studies motivated the development of a numerical model that simulates plucking to explore the evolution of channel profiles in lithologically diverse terrain. In the main governing equation, the incision rate is calculated as a function of the difference between the boundary shear stress and a threshold shear stress needed to entrain blocks from the bed. Because an earlier study suggested that plucking is the primary incisional process in the northern Sierra Nevada (CA), the model was calibrated to approximate the conditions in the region. The profiles of the simulated rivers are stair-stepped, with sharp breaks-in-slope at lithological boundaries. This characteristic is common to rivers draining the northern Sierra Nevada, suggesting that the size of blocks available for plucking, as mediated by the fracture density, may be the primary control on their gradients. Moreover, the numerical experiments highlight the role of threshold shear stresses in the post-orogenic persistence of steep reaches and relict terrain. Finally, comparisons of profiles evolved under tilting or uniform uplift scenarios provide insights into how these different uplift modes affect profile evolution. For example, whereas uniform uplift generates a single migrating knickpoint at the range front, multiple migrating knickpoints can form simultaneously along a river in a tilting landscape. © 2020 John Wiley & Sons, Ltd.

**KEYWORDS:** plucking; river incision; fractures; Sierra Nevada; modelling

## Introduction

The important role of lithology in controlling the slope of bedrock channels has long been recognized (e.g. Hack, 1973 ; Duvall et al., 2004 ; Larue, 2008 ; Cyr et al., 2014). The stream power incision model (SPIM), a common approach to modelling the evolution of bedrock channels, incorporates the resistance of bedrock to erosion with an erodibility term that can be adjusted to account for spatially varying lithologies (e.g. Howard, 1994 ; Forte et al., 2016 ; Perne et al., 2017 ; Yanites et al., 2017). However, as argued in Lague (2014), the SPIM is useful only under a limited set of conditions and more mechanistic models for describing fluvial bedrock incision are needed. A thorough understanding of incisional processes is important as bedrock channel profiles are used to extract information regarding tectonic activity that could be used to assess earthquake hazards (e.g. Merritts and Vincent, 1989 ; Snyder et al., 2000 ; Kirby and Whipple, 2001 ; Pavano et al., 2016).

Advances in our understanding of river incision processes, mainly abrasion and plucking, offer potentially promising improvements over the SPIM (Whipple et al., 2000; Lamb et al., 2015 and references cited therein). Whereas modelling the evolution of channel profiles by abrasion in lithologically diverse terrain is complicated by the role of sediment supply and size (Sklar and Dietrich, 2001), which will vary according to the spatial distribution of lithologies throughout the

watershed, plucking may be a simpler process to model since it depends primarily on local conditions. Therefore, to explore the effects of spatially varying bedrock on the evolution of channel profiles, I introduce a numerical model that incorporates an empirically supported process-based equation describing bedrock channel incision by plucking. This model is based on the theoretical framework developed in previous studies (Chatanantavet and Parker, 2009; Dubinski and Wohl, 2013; Lamb et al., 2015) and is parameterized to approximate conditions in the Sierra Nevada mountains of California, where plucking appears to be the dominant incision process (Whipple et al., 2000) and lithology has a first-order control on channel steepness (Gabet, 2020).

The northern Sierra Nevada marks the location of a subduction zone active during the Jurassic and Cretaceous periods (Snow and Scherer, 2006). As a result of the convergence, this range is lithologically heterogeneous, with a metamorphic belt parallel to the range crest at lower altitudes and plutonic rocks dominating near its crest; moreover, within the metamorphic belt, rock units with a range of erodibilities follow each other in quick succession (Saucedo and Wagner, 1992). The longitudinal profiles of large rivers draining the range and flowing across these lithologies are often composed of approximately straight sections of varying gradients (Figure 1). The breaks-in-slope where the straight sections meet are nearly always at lithological boundaries, providing strong evidence that bedrock

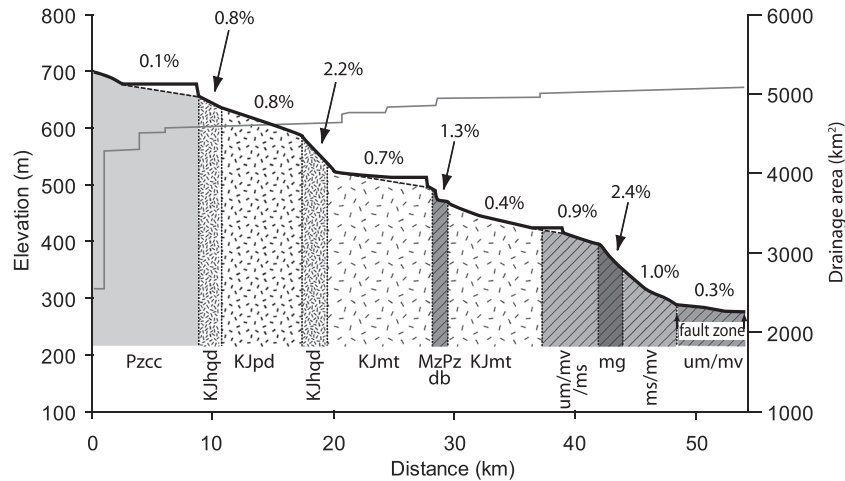


**Figure 1.** Longitudinal profile, surface lithology, and reach gradients along the North Fork Feather River (adapted from Gabet, 2020). Most breaks-in-slope are associated with a lithological transition, strong evidence that lithology exerts a dominant control on reach gradient. Horizontal reaches are reservoirs; inferred bedrock surface shown with dashed line. Pzcc = metachert, argillite; KJhqd = coarse-grained quartz diorite; KJpd = fine- to medium-grained pyroxene diorite; KJmt = coarse-grained monzonite; MzPz db = metabasalt; um = ultramafic; mv = metavolcanic; mg = metagabbro; ms = metasedimentary (Hietanen, 1973; Saucedo and Wagner, 1992). Fill patterns do not represent the subsurface distribution of bedrock. The bottom of the profile is at 39.715°, -121.465°.

erodibility has a dominant control on local channel steepness (Gabet, 2020). Fracture density in the individual bedrock units may have an important role in erodibility by constraining the size of blocks available for plucking (Chatanantavet and Parker, 2009; Scott and Wohl, 2019). A positive relationship between the diameter of the largest in-channel boulders and channel steepness in Sierran rivers also provides evidence for the importance of fracture density in erodibility; indeed, even within the same lithological unit, changes in fracture density are correlated with changes in channel gradient (Gabet, 2020).

With the model parameterized for the northern Sierra Nevada, I performed numerical experiments to investigate the following questions.

*Does a bedrock incision model simulating plucking in lithologically heterogeneous terrain yield stair-stepped river profiles?* The SPIM can be used to evolve stair-stepped profiles (Perne et al., 2017), however, estimating the erodibility constant in the SPIM directly from the characteristics of an individual bedrock unit remains a challenge (Stock et al., 2005). Therefore, a more mechanistic approach that can incorporate field measurements (e.g. fracture density) may be helpful for simulating profile evolution in lithologically complex landscapes.

*Do tilting and uniform uplift leave different topographic signatures on river profiles where plucking dominates?* Tilting and uniform uplift are two end-member descriptions of a 1-D spatial distribution of uplift rates driven by tectonic activity. Uniform uplift via a range-front fault can create a dislocation in a river's profile that migrates upstream as a knickpoint (e.g. Yanites et al., 2010). Uplift by tilting, however, is not accommodated by a range-front fault and, therefore, other landscape features must be used to discern tectonic activity (e.g. Goswami and Pant, 2019). A critical difference between uniform uplift and tilting is that the latter affects the entire drainage network simultaneously, potentially leaving a unique signature on river profiles.

*Can relict terrain persist where plucking dominates?* The plucking of individual blocks from a river's bed requires overcoming a critical shear stress. In the headwater areas of low-relief regions experiencing uplift, the available shear stress may be too low for plucking and the progress of migrating knickpoints may be inhibited (e.g. Baldwin et al., 2003; Brocard et al., 2016). As a result, these headwater regions may persist as relict patches of the original landscape (Twidale, 1998; Bishop and Goldrick, 2010). In the northern Sierra

Nevada, for example, many of the trunk streams originate on high-altitude, low-relief surfaces before plunging down steep cascades and continuing through deep canyons.

*How persistent are post-orogenic profiles where plucking is the dominant incisional process?* In post-orogenic landscapes where channel incision is not limited by a threshold shear stress, bedrock river profiles will decay monotonically (e.g. Baldwin et al., 2003). However, in landscapes where a critical shear stress must be surpassed before incision can proceed, plucking will be suppressed along reaches of rivers that have relaxed below the gradient needed to generate the local critical shear stress. At this point, incision may only occur by other, less-efficient processes such as abrasion, and steep rivers may persist long after the cessation of uplift.

## Methods

### Modelling approach

In the development of this numerical model, I assume that plucking is the sole channel incision process. Furthermore, I assume that block size is a function of fracture density, that fracture density is the only difference between lithological units, and that fracture density (and thus block size) is uniform and isotropic within a single unit (i.e. the blocks are cube-shaped). Moreover, I assume that plucking does not impede the plucking of new blocks but yet there are a sufficient number of large clasts on the bed, from either plucking or slope failures, to affect channel roughness (which may also arise from irregularities in the bed created by the removal of blocks). Note that this model does not account for the transport or comminution of blocks once they are plucked and, therefore, it assumes that the incision rate is solely limited by the rate at which blocks are plucked from the bed.

### Governing equations

The rate at which blocks are plucked from the bed,  $E$  ( $\text{m s}^{-1}$ ), can be expressed as

$$E = (RgD)^{1/2} a_p (\tau^* - \tau_c^*)^{n_p} \quad (1)$$

where  $R = (\rho_r - \rho_w)/\rho_w$  in which  $\rho_r$  and  $\rho_w$  are the density of rock ( $2650 \text{ kg m}^{-3}$ ) and water, respectively;  $g$  is gravitational

acceleration ( $\text{m s}^{-2}$ );  $D$  is block size (m);  $a_p$  and  $n_p$  are dimensionless empirical coefficients with values of 0.02 and 1.5, respectively (Tsujiimoto, 1999);  $\tau^*$  is the dimensionless boundary shear stress; and  $\tau_c^*$  is the dimensionless critical shear stress (Chatanantavet and Parker, 2009; Lamb et al., 2015).

The dimensionless boundary shear stress is determined according to

$$\tau^* = \tau_b / ((\rho_r - \rho_w)gD) \quad (2)$$

where  $\tau_b$  is the boundary shear stress, calculated from

$$\tau_b = \rho_w g (Qn/w)^{0.6} S^{0.7} \quad (3)$$

where  $Q$  is discharge ( $\text{m}^3 \text{s}^{-1}$ ),  $n$  is Manning's roughness coefficient,  $w$  is channel width (m), and  $S$  is slope gradient (Snyder et al., 2003). Peak discharge and channel width are expressed as a function of drainage area ( $A$ ,  $\text{km}^2$ ), and drainage area is determined as a function of river distance from the channel head ( $x$ , km) with data from the northern Sierra Nevada (Gabet, 2020):

$$Q = 1.8A^{0.8} \quad (4)$$

$$w = 10A^{0.20} \quad (5)$$

$$A = 11x^{1.23} \quad (6)$$

Note that the scaling factor in Equation (4) has been adjusted since Gabet (2020) to better represent the discharges during the winter of 2017 on which Equation (5) is based; these data were not available at the time. Note also that channel width does not appear to be sensitive to lithology in the region (Gabet, 2020) and that the potential role of incision rate on cross-sectional geometry is ignored. The few empirical studies that have examined the relationship between channel width and incision rate have yielded contradictory results (Turowski et al., 2009 and references cited therein), and no data exist to evaluate this relationship in the northern Sierra Nevada. The consequence of decoupling channel width from incision rate is that changes in the latter are only accommodated through changes in channel slope (Yanites and Tucker, 2010). Nevertheless, the model presented here could be modified to incorporate a relationship between width and incision rate derived mechanistically (Turowski et al., 2009; Yanites and Tucker, 2010) or empirically (Lague, 2014).

Manning's  $n$  is calculated from (Chow, 1959)

$$n = 0.034D^{1/6} \quad (7)$$

The dimensionless critical shear stress  $\tau_c^*$  is determined according to (Lamb et al., 2015)

$$\tau_c^* = \frac{\cos\theta(\tan\phi - \tan\theta) + 2\tau_w^*}{\left(1 + \frac{1}{2}C_D\left(\frac{u}{u_*}\right)^2\right)\left(1 + F_L^*\tan\phi\right)} \quad (8)$$

where  $\theta$  is the channel slope,  $\phi$  is the friction angle ( $32^\circ$ ),  $\tau_w^*$  is the dimensionless block sidewall stress (0.1),  $C_D$  is a drag coefficient (1),  $u/u_*$  is the ratio of the downstream flow velocity to the shear velocity (8.3),  $P/L$  is the ratio of the protrusion height to the block length (0.2), and  $F_L^*$  is an empirical constant related to the lift force (0.85). The values assigned to the constants are

from Lamb et al. (2015) and are not specific to the Sierra Nevada. With these values, the relationship between the dimensionless critical shear stress and the channel slope can be approximated by

$$\tau_c^* = 0.0873 - 0.1088\tan\theta \quad (9)$$

To scale the entrainment rate [Equation (1)] to an incision rate ( $I$ ,  $\text{mm year}^{-1}$ ) that is meaningful over geologic time, a scaling factor  $k$  is introduced such that

$$I = kE \quad (10)$$

Determining an appropriate value for  $k$  is not straightforward. Because valleys in the northern Sierra Nevada were buried by fluvial and volcanic sediment throughout much of the Cenozoic (Whitney, 1880; Slemmons, 1966), long-term net bedrock incision rates are exceedingly low; for example, Eocene-aged deposits can be found  $<170$  m above the bed of the South Fork American River (Gabet, 2014). Therefore, rather than calibrating  $k$  from field observations,  $k$  is calibrated to yield incision rates that match a specified uplift rate at the range of channel gradients observed in the northern Sierra Nevada (0.1–8.9%) (Gabet, 2020).

Past uplift rates for the northern Sierra Nevada are unknown and the evidence for recent uplift is flawed (Gabet, 2014, 2020), therefore a value of  $0.05 \text{ mm year}^{-1}$  for the modern Andes, a similar convergent margin, is adopted (Evenstar et al., 2015). This rate is used for both the uniform uplift and the tilt scenarios; in the case of the latter, it is the vertical velocity of the highest node (i.e. the crest). With this uplift rate, a value of 0.3 for  $k$  yields gradients similar to those measured in the region.

## Model implementation

The simulated channel is 150 km long, approximately the length of the bedrock portions of the major rivers draining the northern Sierras, and has a node spacing of 50 m. Before uplift, the initial channel profile is described by an exponential function to represent a river draining low-relief terrain (Inoue, 1992); moreover, the initial channel is assumed to be dominated by a long alluvial reach such that its profile is not affected by the underlying bedrock. Two uplift scenarios can be imposed on the initial profile. In the first, the profile is tilted up at a specified rate with the lowest node acting as the tilt axis. In the second, a simulated fault is located 250 m upstream of the lowest node such that all nodes in the profile, except for the five lowest, undergo uniform uplift; to avoid boundary effects, the fault was not placed closer to the end of the channel.

At the beginning of each time step, the gradient is calculated using a centre difference scheme for all of the nodes except those at lithological boundaries; for these, a forward difference scheme is used to preserve sharp breaks-in-slope. The dimensionless shear stress is then calculated at each node [Equation (2)] and compared to that node's dimensionless critical shear stress [Equation (9)]; where  $\tau^* > \tau_c^*$ , Equation (1) is used to calculate the entrainment rate. The entrainment rate is converted to an incision rate [Equation (10)], and the elevation of the node is lowered by the appropriate amount. The elevation of each node is then increased according to the uplift rate. Finally, a smoothing scheme damps numerical instabilities that arise because of the sharp breaks-in-slope at the lithological boundaries with

$$z_i = (bz_{i-1} + z_i + bz_{i+1})/(2b + 1) \quad (11)$$

where  $z$  is elevation (m),  $b$  is a weighting coefficient and  $i$  is a



spatial indexing term. A value of 0.18 for  $b$  was found to be sufficient to prevent the growth of instabilities. To preserve the breaks-in-slope, this scheme was not applied to nodes at lithological boundaries. Finally, all of the model runs were halted before the migrating knickpoints could reach the end of the simulated profile. In exploratory model runs, the headwater region would steepen beyond gradients ( $>10\%$ ) where incision by fluvial processes may not be relevant (Stock and Dietrich, 2003).

## Analytical solution

An analytical steady-state (i.e.  $E = U$ ) solution to Equation (1) is obtained by combining it with Equation (10) to produce.

$$U = k(RgD)^{1/2} a_p (\tau^* - \tau_c^*)^{n_p} \quad (12a)$$

which can be rewritten as

$$\tau^* = \tau_c^* + \left[ \frac{U}{ka_p(RgD)^{1/2}} \right]^{2/3} \quad (12b)$$

Substituting the standard equation for the boundary shear stress ( $\tau_b = \rho ghS$ , where  $h$  is flow depth) into Equation (2), inserting Equation (2) into Equation (12b), and solving for slope yields

$$S = \frac{1.65D}{h} \left[ \tau_c^* + \left( \frac{U}{ka_p(RgD)^{1/2}} \right)^{2/3} \right] \quad (13)$$

Rewriting Manning's equation (Snyder et al., 2003) as

$$h = \left( \frac{Qn}{w} \right)^{3/5} S^{-3/10} \quad (14)$$

and inserting it into Equation (13) leads to

$$S = \left[ 1.65D \left( \frac{Qn}{w} \right)^{-3/5} \left( \tau_c^* + \frac{U}{ka_p(RgD)^{1/2}} \right)^{2/3} \right]^{10/7} \quad (15)$$

Because  $S = \Delta z / \Delta x$ , Equation (15) can be used to calculate the elevations along a steady-state longitudinal profile with the relationships expressed by Equations (4)–(7). Note, however, that this approach requires the use of a constant  $\tau_c^*$ ; for the range of slopes modelled here, a value of 0.077 is appropriate [Equation (9)].

The analytical solution was derived to evaluate whether the smoothing algorithm and the mixing of finite difference schemes affect the results from the numerical model. Comparisons of the two approaches revealed negligible differences in the profiles, particularly at the lithological transitions where the mixed finite difference schemes might have had the biggest effects.

## Caveats

As with all numerical models, the one presented here comes with caveats. First, although Equation (1) represents plucking by both vertical entrainment and sliding, each process requires a different critical shear stress (Dubinski and Wohl, 2013; Lamb et al., 2015). My observations (albeit limited) suggest that sliding is the dominant plucking process in the northern Sierra Nevada, particularly in the granitic bedrock. For example, reaches often have bedrock steps that appear to be controlled by joint sets such that blocks at the front of the steps can be dislodged by sliding (Figure 2); in addition, cavities left behind by vertically plucked blocks are rare. Therefore, the lower critical shear stress for sliding is adopted here; however, because sliding blocks need a downhill face free of obstructions, plucking by vertical entrainment may occasionally be necessary to initiate the process of incision by sliding. Nevertheless, to reduce the number of unconstrained parameters, this process is not explicitly modelled. The second limitation is that, although incision equations that incorporate an excess shear-stress term are sensitive to the distribution of discharges (Snyder et al., 2003), I use only a single discharge–area relationship. Similarly, I assume that the climate is unvarying over the tens of millions of years of model time. Because the focus of this study is a general understanding of how a plucking model can be used to simulate the evolution of bedrock profiles, I consider these simplifications to be adequate. Third, the channel is assumed to be straight and aligned directly down the dip of the uplifting terrain. In reality, the major bedrock rivers draining the northern Sierra Nevada have somewhat meandering planforms and, therefore, when tilted, the tilt rate of each reach would depend on its azimuth. Fourth, although the supply of large clasts from adjacent hillslopes in mountainous terrain may affect the evolution of river profiles (Shobe et al., 2016, 2018; DiBiase et al., 2018), this process is not accounted for here. Fifth, Chatanantavet and Parker (2009) suggest that fracture density along the bed of a bedrock channel may increase through time such that the diameter of blocks available for plucking is partially dependent on incision rate. Although incorporating an ‘aging’ function would be interesting because of potential negative feedbacks between erodibility and incision rate, I did not implement one due to the lack of data needed for calibration.

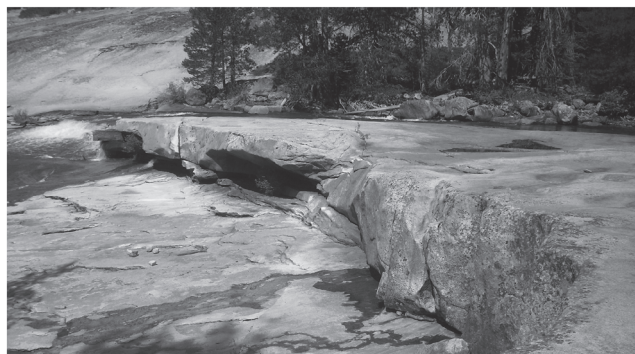


**Figure 2.** Echo Creek (Yosemite National Park) at low flow. Plucking at the bedrock step (~ 60 cm high) occurs by the downstream sliding of blocks along an exfoliation joint.

Moreover, a different aging function would likely be needed for each bedrock unit. Finally, the goal of these numerical experiments is not to reproduce specific profiles in the northern Sierra Nevada but, rather, this region is used as a test bed for exploring profile evolution in plucking-dominated landscapes with spatially varying erodibility thresholds.

## Results and Discussion

### The evolution of stepped profiles

In this experiment, I modelled both tilting and uniform uplift for a landscape characterized by alternating bands of weak (i.e. small blocks) and resistant (i.e. large blocks) lithologies with weak bedrock beginning the sequence at the base of the profile. In both tectonic scenarios, the profile after 40 Ma was stepped: steep reaches formed in bedrock with large blocks available for plucking and gentler reaches formed in bedrock with smaller blocks (Figures 3 and 4). The modelled profiles are similar to those of northern Sierran rivers: reach gradient varies according to erodibility and there are sharp breaks-in-slope at the lithological boundaries (Figure 1). Although Perne et al. (2017) developed stair-stepped profiles in lithologically heterogeneous terrain using the SPIM, the results presented here indicate that a model which simulates plucking provides sufficient conditions for evolving this type of profile as well. The formation of knickpoints at the lithological boundaries highlights the importance of accounting for differences in bedrock when using river profiles and knickpoints to infer tectonic activity (e.g. Duvall et al., 2004 ; Pavano et al., 2016 ; Yanites et al., 2017). Indeed, as noted in Gabet (2020), some studies in the Sierra Nevada have mistaken lithologically controlled

changes in channel slope for evidence supporting tectonic activity. Accounting for differences in erodibility should be particularly important in convergent orogens, where bands of different rocks may be aligned perpendicular to the regional slope such that large rivers draining the range cross multiple lithologies. In addition, the specific pattern of erodibility influences how quickly the profile reaches steady-state conditions when tilted: after 40 Ma, the first 40 km of the profile with a more erodible lithology at the base has reached steady state (Figure 3), whereas there are no steady-state reaches in a profile with a more resistant base (Figure 5).

### Different signatures of tilting vs. uniform uplift

Tilting was imposed on a landscape in which the alternating bands of rock began with resistant rock at the base of the tilting profile; the result suggests that knickpoints can initiate anywhere along the profile where the bedrock is more erodible and not necessarily at the range front (Figure 5). In contrast, under the uniform uplift scenario, a migrating knickpoint only initiates at the range front where faulting introduces a dislocation at a single point in the profile (Figure 4). Because tilting simultaneously increases the slope of the entire river, the shear stress may overcome the critical shear stress along different individual reaches with erodible bedrock, thereby initiating multiple knickpoints upstream of the tilt axis. Therefore, in addition to the problem of distinguishing uplift-generated breaks-in-slope from those created by lithological transitions (e.g. Hack, 1957 ; Lecce, 1997 ; Duvall et al., 2004 ; Phillips and Lutz, 2008 ; Pike et al., 2010 ; Gabet, 2020), tilting may further complicate attempts to infer discrete pulses of uplift from bedrock river profiles in lithologically diverse terrain.

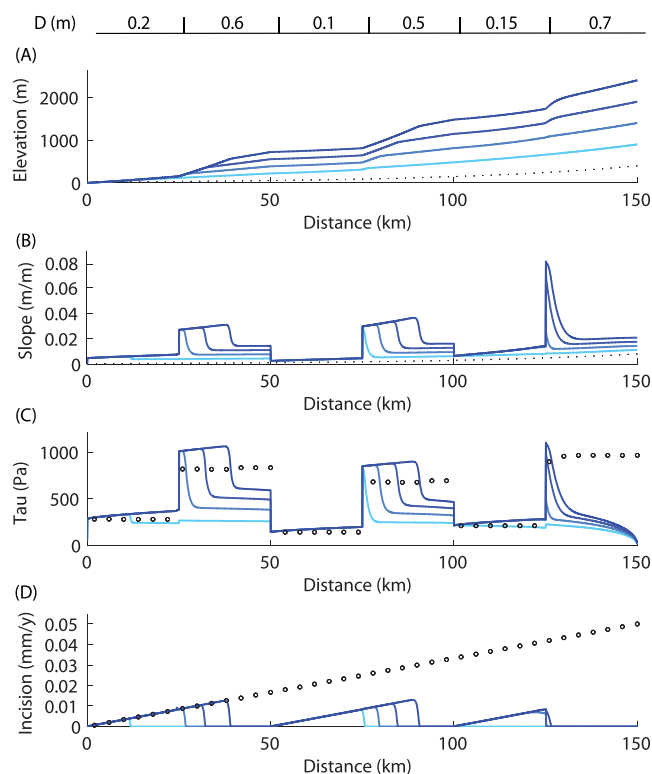


**Figure 3.** Profile evolution in a tilting landscape underlain by heterogeneous bedrock. Distribution of block sizes shown at top. Different lines in each plot represent model state at 10 Ma intervals with colours becoming darker with time. (A) Initial profile shown with dotted line. As the landscape tilts, breaks-in-slope form at the lithological boundaries. (B) Initial slopes shown with dotted line. Reaches underlain by resistant rock steepen relative to reaches underlain by weaker rock. (C) Critical shear stress shown with dotted lines. (D) Steady-state incision rate shown with dotted line. Three migrating knickpoints have formed independently; however, only the one at the range front has generated steady-state incision rates. [Colour figure can be viewed at [wileyonlinelibrary.com](http://wileyonlinelibrary.com)]

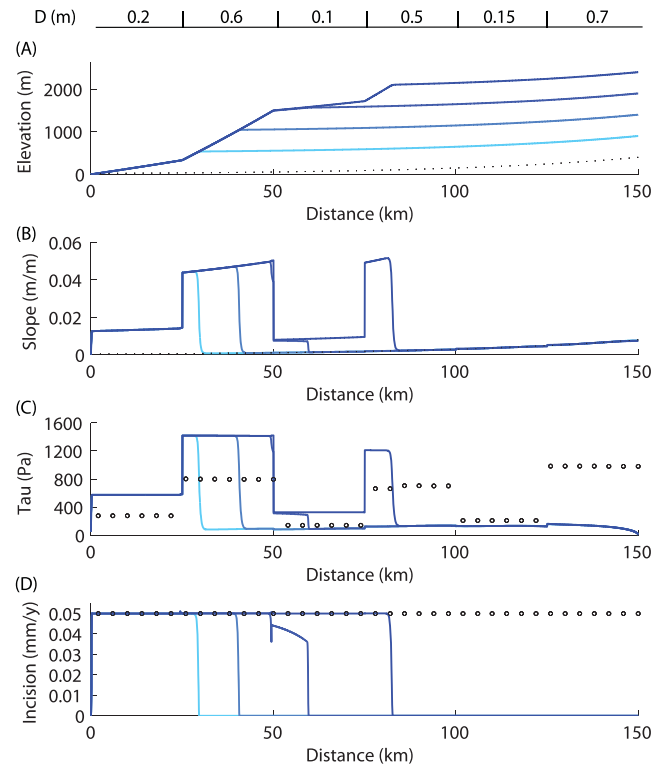


**Figure 4.** Profile evolution in a lithologically heterogeneous landscape undergoing uniform uplift. The symbology and block sizes are identical to Figure 2. (A) As the landscape is uplifted, a knickpoint generated at the range front sweeps up the channel, leaving in its wake channel reaches adjusted to bedrock erodibility. (B) Channel slopes vary according to erodibility. (C) The excess shear stress is higher than under the tilting scenario (Figure 3) because the uplift rate in the latter decreases towards the tilt axis. (D) In contrast to the tilting scenario, steady-state conditions have advanced further up the profile. [Colour figure can be viewed at [wileyonlinelibrary.com](http://wileyonlinelibrary.com)]

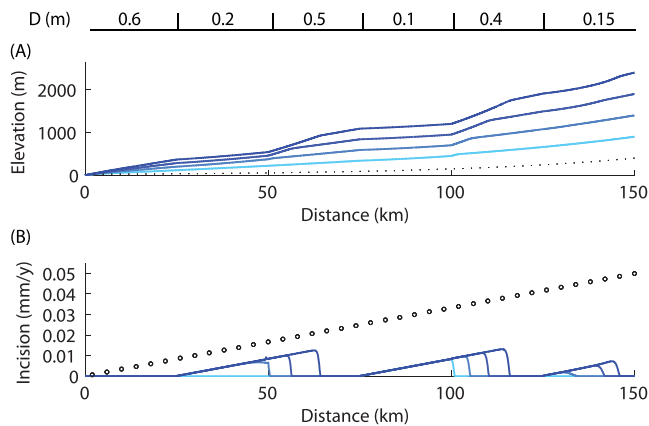


**Figure 5.** Profile evolution where a band of resistant rock lines the range front in a tilting landscape. The symbology is identical to Figure 2. (A) As in the other simulations, a stair-stepped profile develops over time. (B) Knickpoints have initiated in the weak bedrock far from the range front and propagated into the stronger bedrock. If the simulation is run for longer than 40 Ma, the entire profile eventually reaches steady state. [Colour figure can be viewed at [wileyonlinelibrary.com](http://wileyonlinelibrary.com)]

Another difference between profiles in tilting landscapes and those undergoing uniform uplift can be found in the headwaters region not yet affected by knickpoints migrating from downstream. This difference is particularly clear where the high-elevation section of the river is in resistant bedrock. Under the tilting scenario, the relict headwaters region has gradually accumulated tilt since the onset of uplift (Figure 3) because the slopes have not sufficiently steepened to trigger incision that would remove the accumulated tilt; in the uniform uplift scenario, however, the relict portion of the landscape retains

its initial slope (Figure 4). Therefore, if field observations can be used to constrain a channel's pre-uplift slope, these model results could help to distinguish the dominant nature of the uplift.

The spatial distribution of bedrock incision rates along the profile could also be used to discern the nature of the uplift. In the case of uniform uplift, a knickpoint initiating at the range front and migrating upstream leaves uniform rates of bedrock incision in its wake (Figure 4). In contrast, in the tilted landscape, incision initiates where the rock is more erodible, creating a highly non-uniform pattern of incision rates before steady-state conditions are achieved (Figure 3). Therefore, these two uplift modes could be distinguished by measuring long-term incision rates in weak and resistant lithologies (distinguishable by reach gradient): uniform rates would suggest uniform uplift, and higher rates in weaker lithologies, relative to the resistant rocks, would suggest uplift by tilting. In addition, under steady-state conditions, incision rates in a tilting landscape should increase upstream as points further away from the tilt axis experience progressively greater uplift rates.

### The persistence of post-orogenic profiles

In these simulations, the uplift rate was set to zero after 40 Ma of uplift, and the profiles were allowed to decay. In both the tilting and uniform uplift scenarios, the gradients of the reaches generally decrease after the cessation of uplift (Figures 6 and 7). However, once a section of river reaches its critical gradient (i.e. the minimum gradient needed to generate the critical shear stress), incision stops. Of course, in reality, other incision processes, such as abrasion, would continue to operate; however, where plucking is the dominant process, these other processes

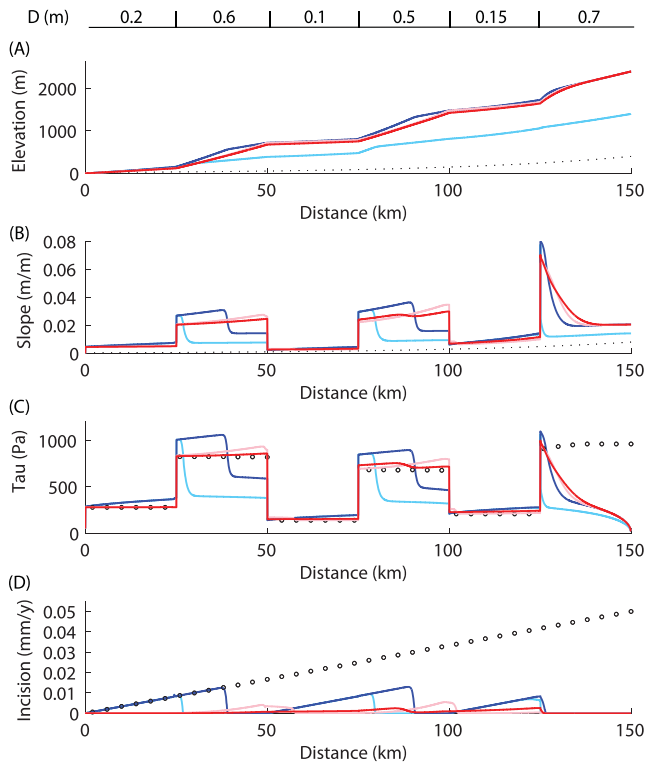


**Figure 6.** Profile evolution in a tilting landscape during and after uplift. Each line represents the model state after 20 Ma; blue = uplift phase, red = post-orogenic phase. Meaning of dotted lines same as previous figures. (A) The post-orogenic profile has not cut down significantly relative to the uplift profile because the shear stresses during the uplift phase were only slightly higher than the critical shear stresses (C). (B) Slopes decrease post-orogenically in the wake of knickpoints migrating through the resistant reaches. (D) Dissipation of knickpoints against the more resistant units can be seen in the spatial distribution of incision rates. [Colour figure can be viewed at [wileyonlinelibrary.com](http://wileyonlinelibrary.com)]

will be less effective (by definition) and, as a result, post-orogenic profiles may be remarkably persistent.

Another similarity between the two tectonic scenarios is the post-orogenic fate of the migrating knickpoints. In both cases, migrating knickpoints fade during their passage into a band of resistant rock at the top of the profile as the slope of the knickpoint relaxes down to the critical gradient and the shear stresses become too low to dislodge blocks from the bed. As a result of the knickpoint's dissipation, the relict landscapes in the upper reaches of the watersheds become persistent features.

These two experiments also highlight the controls on reach gradient during and after uplift, particularly in the uniform uplift scenario (Figure 7). During uplift, reaches steepen until their erosion rates match the uplift rate; the uplift rate, therefore, sets a bound on the maximum gradient of each reach. After the cessation of uplift, the slope of each reach declines to its critical gradient; block size, therefore, sets a bound on a reach's minimum gradient. This distinction can be appreciated by rewriting Equation (13) as

$$S = \frac{1.65D}{h} \tau_c^* + \frac{1.65D}{h} \left( \frac{U}{ka_p(Rgd)^{1/2}} \right)^{2/3} \quad (16)$$

to isolate the two additive components of reach gradient. The first term on the right-hand side (RHS) is the critical gradient and the second term on the RHS is the additional increment of slope needed for incision to match the uplift rate. Thus, at

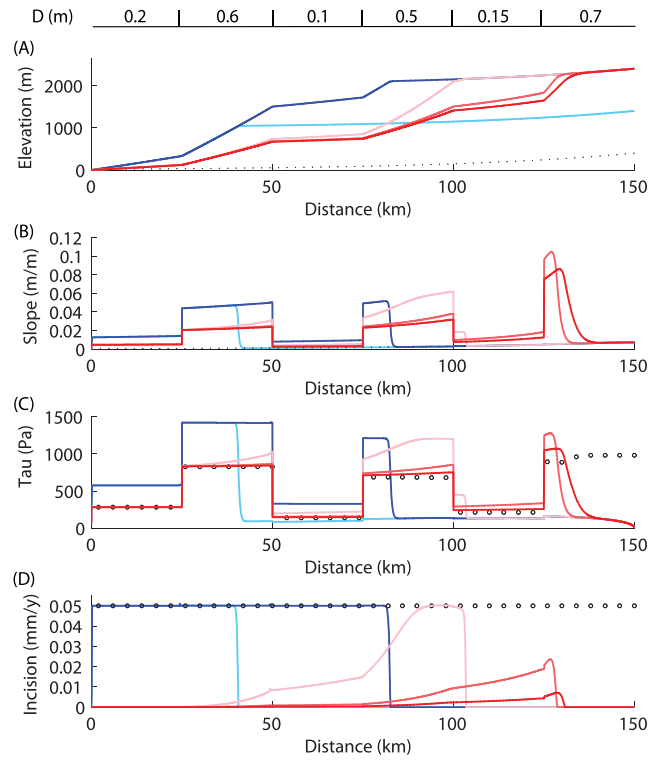


**Figure 7.** Profile evolution during and after uniform uplift. The symbology is identical to Figure 6. (A) The final post-orogenic profile is substantially different from the uplift profile because steady-state conditions were attained along most of the river's length (D). However, once the critical gradients are reached, the profile becomes nearly static. (B) The decline in gradient is greater in the steep reaches than the gentle reaches because the steady-state excess shear stress is greater in the reaches underlain by more resistant rock (C). (D) Dissipation of the knickpoint against the more resistant unit can be seen in the spatial distribution of incision rates. [Colour figure can be viewed at [wileyonlinelibrary.com](http://wileyonlinelibrary.com)]

steady state, reach slopes will be the sum of both terms on the RHS while, in post-orogenic situations (i.e.  $U = 0$ ), reach slopes will decline down to the critical gradient. Moreover, according to Equation (16), uplift exerts the dominant control on reach slope as uplift rates increase above  $\sim 0.01 \text{ mm year}^{-1}$  (Figure 8) and beyond  $0.1 \text{ mm year}^{-1}$ , the contribution of the critical gradient to the overall slope becomes negligible.

An important consequence of an incision process like plucking is that it sets a topographic and climatic threshold below which incision stops (or slows dramatically in the real world) (e.g. Baldwin et al., 2003). A river's profile, therefore, may persist if the slopes of its reaches match or fall below the critical gradient or if peak discharges decrease due to climatic changes. As noted earlier, Eocene–Early Oligocene fluvial sediment can be found within 100–200 m of the modern river beds in deep canyons in the Sierra Nevada (Gabet, 2014). These deposits indicate that the profiles of these rivers are long-lived and attest to very low net incision rates over much of the Cenozoic. Burial of the river beds by fluvial and volcanic deposits over this time period is undoubtedly partially responsible for these low rates of bedrock incision (Gabet, 2014); however, a decline in available shear stresses due to regional decreases in precipitation since the Eocene (Chamberlain et al., 2012) and truncation of the headwaters (Schweikert, 2009) may also be responsible.

Investigating changes in reach gradient during and after uplift is also relevant for understanding the effect of lithological heterogeneity in the evolution of mountainous topography. Under post-orogenic conditions, spatial variations in erodibility can lead to differential erosion whereby areas underlain by weaker rock erode more quickly than those underlain by more resistant



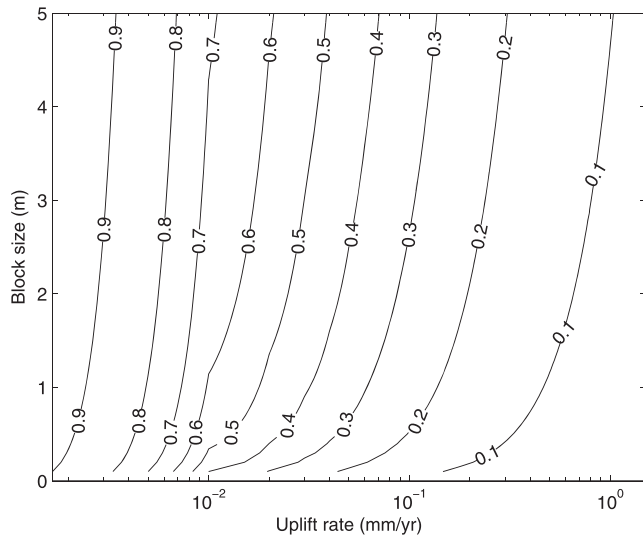


**Figure 8.** Ratio of the critical gradient to the reach gradient under steady-state conditions calculated with Equation (16). At low uplift rates, reach gradient is primarily dependent on block size; however, as the uplift rate increases, the importance of the critical shear stress declines. Note the logarithmic scale on the x-axis.

rock (e.g. Jansen et al., 2010). Accordingly, Gabet (2020) proposed that, in the Sierra Nevada, post-orogenic differential erosion had amplified the differences in the gradients of reaches underlain by rocks of different erodibilities. The numerical experiments presented here suggest otherwise: in the sections of river that were at or near steady state, the difference in gradients between reaches of different erodibilities *decreases* post-orogenically (Figures 6 and 7). Because the incision rate is proportional to the excess shear stress [Equation (1)], a reach with a higher critical shear stress will need to increase its slope by a greater amount than one with a lower critical shear stress to incise at a rate equal to the uplift rate. Therefore, after the cessation of uplift, a less erodible reach will experience a greater decrease in gradient than a more erodible reach as they both relax down to their critical slope.

## The persistence of relict terrain

In this simulation, uniform uplift was imposed for 40 Ma on a model space underlain by uniform lithology that produces 0.8-m blocks. After 40 Ma, uplift was set to zero and the profiles evolved for an additional 80 Ma. After the cessation of uplift, the knickpoint continues to migrate upstream, albeit at a progressively slower rate as gradients approach the critical slope (Figure 9). Eventually, shear stresses match or fall below the critical shear stress and the knickpoint's upstream progress is arrested, preserving the headwaters region of the river as a relict patch of the initial landscape. Thus, even in the absence of lithologically heterogeneous bedrock, relict terrain can persist in plucking-dominated landscapes (see also Baldwin et al., 2003).

## Conclusions

Although some of the results presented here have already been simulated with the SPIM, the SPIM has deficiencies that could potentially be overcome through the adoption of approaches that are more faithful to the physics of the incision processes. (Lague, 2014) The plucking model used in this study may represent a step towards that goal. For example, simulations of

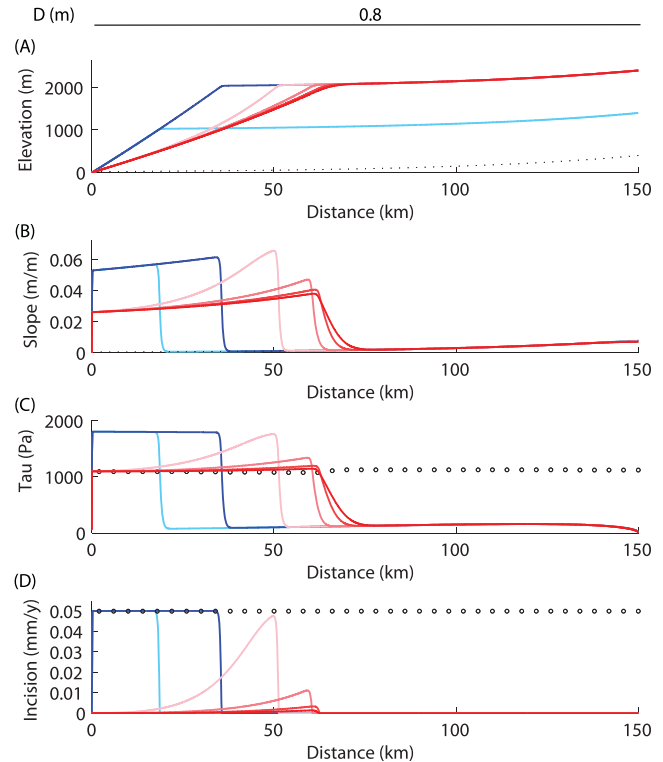


**Figure 9.** Post-orogenic relict landscape in uniform lithology. The symbology is identical to Figure 6, except that each line represents the profile after 20 Ma. (A) After the cessation of uplift, the profile declines while the knickpoint progressively slows and then stops, thereby preserving a portion of the initial landscape. (B) After the cessation of uplift, the gradients decrease until the shear stress matches the critical shear stress (C). (D) Incision rates decline as the knickpoint dissipates. The incision advances like a front during uplift but like a wave in post-orogenic conditions. [Colour figure can be viewed at [wileyonlinelibrary.com](http://wileyonlinelibrary.com)]

incision through rock types with different fracture densities evolve longitudinal profiles that bear strong resemblances to profiles in the northern Sierra Nevada, a lithologically diverse landscape. Specifically, both are composed of approximately straight links, of varying slopes, that meet at lithological boundaries to form knickpoints. These numerical experiments demonstrate that accounting for spatial variations in threshold shear stresses on channel gradient is critical when inferring tectonic activity from river profiles, particularly in convergent tectonic environments, and they affirm the importance of these thresholds in the persistence of post-orogenic river profiles and the preservation of relict terrain where plucking dominates. In addition, to the extent that fracture density controls the size of blocks available for plucking, this analysis suggests the potential for the direct field measurement of a landscape metric that can be used to estimate erodibility, a task that is more challenging with other approaches. Moreover, the results highlight important differences between bedrock profiles developed in tilting terrain and those formed under conditions of uniform uplift, including the location of knickpoint generation and the evolution of the profiles after the cessation of uplift. Finally, this study emphasizes the need, as others have done elsewhere (e.g. Scott and Wohl, 2019), to understand the controls on fracturing of bedrock at the Earth's surface. In regions where channel incision is dependent on fracture density, the rate of fracture formation and propagation may limit the pace of landscape evolution.

**Acknowledgements**—Dan Scott, an anonymous reviewer, and the Editor are thanked for their generous and helpful comments.



## Data Availability Statement

The Matlab code for this model is available by contacting the author at [manny.gabet@sjsu.edu](mailto:manny.gabet@sjsu.edu).

## Conflict of Interest Statement

The author declares that there are no conflicts of interest.

## References

- Baldwin JA, Whipple K, Tucker GE. 2003. Implication of the shear stress incision model for the timescale of postorogenic decay of topography. *Journal of Geophysical Research, B: Solid Earth* **108**: 1–17.
- Bishop P, Goldrick G. 2010. Lithology and the evolution of bedrock rivers in post-orogenic settings: constraints from the high-elevation passive continental margin of SE Australia. In *Australian Landscapes*, Bishop P, Pillans B (eds). Geological Society: London; 267–287.
- Brocard GY, Willenbring JK, Miller TE, Scatena FN. 2016. Relict landscape resistance to dissection by upstream migrating knickpoints. *Journal of Geophysical Research - Earth Surface* **121**: 1182–1203. <https://doi.org/10.1002/2015JF003678>.
- Chamberlain CP, Mix HT, Mulch A, Hren MT, Kent-Corson ML, Davis SJ, Horton T, Graham SA. 2012. The Cenozoic climatic and topographic evolution of the western North American Cordillera. *American Journal of Science* **312**: 213–262. <https://doi.org/10.2475/02.2012.05>.
- Chatanantavet P, Parker G. 2009. Physically based modeling of bedrock incision by abrasion, plucking, and macroabrasion. *Journal of Geophysical Research - Earth Surface* **114**: 1–22. <https://doi.org/10.1029/2008JF001044>.
- Chow VT. 1959. *Open Channel Hydraulics*. McGraw-Hill: New York.
- Cyr AJ, Granger DE, Olivetti V, Molin P. 2014. Distinguishing between tectonic and lithologic controls on bedrock channel longitudinal profiles using cosmogenic <sup>10</sup>Be erosion rates and channel steepness index. *Geomorphology* **209**: 27–38.
- DiBiase RA, Rossi MW, Neely AB. 2018. Fracture density and grain size controls on the relief structure of bedrock landscapes. *Geology* **46**: 399–402. <https://doi.org/10.1130/g40006.1>.
- Dubinski IM, Wohl EE. 2013. Relationships between block quarrying, bed shear stress, and stream power: a physical model of block quarrying of a jointed bedrock channel. *Geomorphology* **180**: 66–81.
- Duvall AR, Kirby E, Burbank DW. 2004. Tectonic and lithologic controls on bedrock channel profiles and processes in coastal California. *Journal of Geophysical Research* **109**: 1–18. <https://doi.org/10.1029/2003JF000086>.
- Evenstar LA, Stuart FM, Hartley AJ, Tattich B. 2015. Slow Cenozoic uplift of the western Andean Cordillera indicated by cosmogenic <sup>3</sup>He in alluvial boulders from the Pacific Planation Surface. *Geophysical Research Letters* **42**: 8448–8455.
- Forte AM, Yanites BJ, Whipple KX. 2016. Complexities of landscape during incision through layered stratigraphy with contrasts in rock strength. *Earth Surface Processes and Landforms* **41**: 1736–1757.
- Gabet EJ. 2014. Late Cenozoic uplift of the Sierra Nevada, California? A critical analysis of the geomorphic evidence. *American Journal of Science* **314**: 1224–1257. <https://doi.org/10.2475/08.2014.03>.
- Gabet EJ. 2020. Lithological and structural controls on river profiles and networks in the northern Sierra Nevada. *Geological Society of America Bulletin*. in press. <https://doi.org/10.1130/B35128.1>.
- Goswami PK, Pant S. 2019. Active bidirectional tectonic-tilting in a part of the Almora klippe, Kumaun Lesser Himalaya, India: insights from statistical analyses of geomorphic indices. *Quaternary International* **523**: 46–53.
- Hack JT. 1957. Studies of longitudinal profiles in Virginia and Maryland. *USGS Professional Paper* **294-B**: 45–97.
- Hack JT. 1973. Stream-profile analysis and stream-gradient index. *Journal of Research of the U.S. Geological Survey* **1**: 421–429.
- Hietanen A. 1973. Geology of the Pulga and Bucks Lake Quadrangles, Butte and Plumas Counties, California. USGS Professional Paper 731; 66.
- Howard AD. 1994. A detachment-limited model of drainage basin evolution. *Water Resources Research* **30**: 2261–2285.
- Inoue K. 1992. Downstream change in grain size of river bed sediments and its geomorphological implications in the Kanto Plain, central Japan. *Geographical Review Japan* **65**: 75–89.
- Jansen JD, Codilean AT, Bishop P, Hoey TB. 2010. Scale dependence of lithological control on topography: bedrock channel geometry and catchment morphometry in western Scotland. *Journal of Geology* **118**: 223–246.
- Kirby E, Whipple KX. 2001. Quantifying differential rock-uplift rates via stream profile analysis. *Geology* **29**: 415–418.
- Lague D. 2014. The stream power river incision model: evidence, theory and beyond. *Earth Surface Processes and Landforms* **39**: 38–61.
- Lamb MP, Finnegan NJ, Scheingross JS, Sklar LS. 2015. New insights into the mechanics of fluvial bedrock erosion through flume experiments and theory. *Geomorphology* **244**: 33–55.
- Larue J-P. 2008. Effects of tectonics and lithology on long profiles of 16 rivers of the south Central Massif border between the Aude and the Orb (France). *Geomorphology* **93**: 343–367.
- Lecce SA. 1997. Nonlinear downstream changes in stream power on Wisconsin's Blue River. *Annals of the Association of American Geographers* **87**: 471–486.
- Merritts D, Vincent KR. 1989. Geomorphic response of coastal streams to low, intermediate, and high rates of uplift, Medocino triple junction region, northern California. *GSA Bulletin* **101**: 1373–1388.
- Pavano F, Pazzaglia FJ, Catalano S. 2016. Knickpoints as geomorphic markers of active tectonics: a case study from northeastern Sicily (southern Italy). *Lithosphere* **8**: 633–648.
- Perne M, Covington MD, Thaler EA, Myre JM. 2017. Steady state, erosional continuity, and the topography of landscapes developed in layered rocks. *Earth Surface Dynamics* **5**: 85–100.
- Phillips JD, Lutz JD. 2008. Profile convexities in bedrock and alluvial streams. *Geomorphology* **102**: 554–566.
- Pike AS, Scatena FN, Wohl EE. 2010. Lithological and fluvial controls on the geomorphology of tropical montane stream channels in Puerto Rico. *Earth Surface Processes and Landforms* **35**: 1402–1417.
- Saucedo GJ, Wagner DL. 1992. *Geologic map of the Chico quadrangle*. California Division of Mines and Geology: San Francisco, CA.
- Schweikert RA. 2009. Beheaded west-flowing drainages in the Lake Tahoe region, northern Sierra Nevada: implications for timing and rates of normal faulting, landscape evolution and mechanism of Sierran uplift. *International Geology Review* **51**: 994–1033.
- Scott DN, Wohl EE. 2019. Bedrock fracture influences on geomorphic process and form across process domains and scales. *Earth Surface Processes and Landforms* **44**: 27–45.
- Shobe CM, Tucker GE, Anderson RS. 2016. Hillslope-derived blocks retard river incision. *Geophysical Research Letters* **43**: 5070–5078.
- Shobe CM, Tucker GE, Rossi MW. 2018. Variable-threshold behavior in rivers arising from hillslope-derived blocks. *Journal of Geophysical Research - Earth Surface* **123**: 1931–1957.
- Sklar LS, Dietrich WE. 2001. Sediment and rock strength controls on river incision into bedrock. *Geology* **29**: 1087–1090.
- Slemmons DB. 1966. Cenozoic volcanism of the central Sierra Nevada, California. In *Geology of Northern California*, Bailey EH (ed). San Francisco: California Division of Mines and Geology Bulletin; 199–208.
- Snow CA, Scherer H. 2006. Terranes of the western Sierra Nevada Foot-hills metamorphic belt, California: a critical review. *International Geology Review* **48**: 46–62.
- Snyder N, Whipple KX, Tucker G, Merritts D. 2000. Landscape response to tectonic forcing: DEM analysis of stream profiles in the Mendocino triple junction region, northern California. *Geological Society of America Bulletin* **112**: 1250–1263.
- Snyder NP, Whipple KX, Tucker GE, Merritts DJ. 2003. Importance of a stochastic distribution of floods and erosion thresholds in the bedrock river incision problem. *Journal of Geophysical Research* **108**: 1–14.
- Stock JD, Dietrich WE. 2003. Valley incision by debris flows: evidence of a topographic signature. *Water Resources Research* **39**: 1–25. <https://doi.org/10.1029/2001WR001057>.
- Stock JD, Montgomery DR, Collins BD, Dietrich WE, Sklar L. 2005. Field measurements of incision rates following bedrock exposure: implications for process controls on the long profiles of valleys cut

- by rivers and debris flows. *Geological Society of America Bulletin* **117**: 174–194.
- Tsujimoto T. 1999. Sediment transport processes and channel incision: mixed size sediment transport, degradation and armoring. In *Incised River Channels*, Darby SE, Simon A (eds). John Wiley: Hoboken, NJ; 37–66.
- Turowski JM, Lague D, Hovius N. 2009. Response of bedrock channel width to tectonic forcing: insights from a numerical model, theoretical considerations, and comparison with field data. *Journal of Geophysical Research - Earth Surface* **114**: 1–16.
- Twidale CR. 1998. Antiquity of landforms: an 'extremely unlikely' concept vindicated. *Australian Journal of Earth Sciences* **45**: 657–668.
- Whipple KX, Hancock GS, Anderson RS. 2000. River incision into bedrock: mechanics and relative efficacy of plucking, abrasion, and cavitation. *Geological Society of America Bulletin* **112**: 490–503.
- Whitney JD. 1880. *The Auriferous Gravels of the Sierra Nevada of California*. Cambridge University Press: Cambridge.
- Yanites BJ, Tucker GE. 2010. Controls and limits on bedrock channel geometry. *Journal of Geophysical Research - Earth Surface* **115**: 1–17.
- Yanites BJ, Tucker GE, Mueller KJ, Chen Y-G. 2010. How rivers react to large earthquakes: evidence from central Taiwan. *Geology* **38**: 639–642.
- Yanites BJ, Becker JK, Madritsch H, Schnellmann M, Ehlers TA. 2017. Lithologic effects on landscape response to base level changes: a modeling study in the context of the Eastern Jura Mountains, Switzerland. *Journal of Geophysical Research - Earth Surface* **122**: 2196–2222.